

Low thermal expansion and broad band photoluminescence of $Zr_{0.1}Al_{1.9}Mo_{2.9}V_{0.1}O_{12}$

Jun-Ping Wang(王俊平), Qing-Dong Chen(陈庆东), Li-Gang Chen(陈立刚), Yan-Jun Ji(纪延俊), You-Wen Liu(刘友文), and Er-Jun Liang(梁二军)

Citation: Chin. Phys. B, 2021, 30 (**3**): 036501. DOI: 10.1088/1674-1056/abcf39
Journal homepage: http://cpb.iphy.ac.cn; http://iopscience.iop.org/cpb

What follows is a list of articles you may be interested in

Laser scattering, transmittance and low thermal expansion behaviors in $Y_{2-x}(ZnLi)_xMo_3O_{12}$ by forming regular grains

Xian-Sheng Liu(刘献省), Yong-Guang Cheng(程永光), Bao-He Yuan(袁保合), Er-Jun Liang(梁二军), Wei-Feng Zhang(张伟风)

Chin. Phys. B, 2019, 28 (**9**): 096501. DOI: 10.1088/1674-1056/ab3435

Conductive property of $Zr_{0.1}Fe_{0.9}V_{1.1}Mo_{0.9}O_7$ with low thermal expansion

Xiaoke He(何小可), Heng Qi(戚恒), Qi Xu(徐启), Xiansheng Liu(刘献省), Lei Xu(许磊), Baohe Yuan(袁保合)

Chin. Phys. B, 2019, 28 (**5**): 056501. DOI: 10.1088/1674-1056/28/5/056501

Phase transition and near-zero thermal expansion of $Zr_{0.5}Hf_{0.5}VPO_7$

Jun-Ping Wang(王俊平), Qing-Dong Chen(陈庆东), Sai-Lei Li(李赛磊), Yan-Jun Ji(纪延俊), Wen-Ying Mu(穆文英), Wei-Wei Feng(冯伟伟), Gao-Jie Zeng(曾高杰), You-Wen Liu(刘友文), Er-Jun Liang(梁二军)

Chin. Phys. B, 2018, 27 (**6**): 066501. DOI: 10.1088/1674-1056/27/6/066501

Near-zero thermal expansion of $In_{2(1-x)}(HfMg)_xMo_3O_{12}$ with tailored phase transition

Yong-Guang Cheng(程永光), Yan-Chao Mao(毛彦超), Xain-Sheng Liu(刘献省), Bao-He Yuan(袁保合), Ming-Ju Chao(晁明举), Er-Jun Liang(梁二军)

Chin. Phys. B, 2016, 25 (**8**): 086501. DOI: 10.1088/1674-1056/25/8/086501

Phase transition and thermal expansion property of $Cr_{2-x}Zr_{0.5x}Mg_{0.5x}Mo_3O_{12}$ solid solution

Song Wen-Bo, Wang Jun-Qiao, Li Zhi-Yuan, Liu Xian-Sheng, Yuan Bao-He, Liang Er-Jun

Chin. Phys. B, 2014, 23 (**6**): 066501. DOI: 10.1088/1674-1056/23/6/066501

Low thermal expansion and broad band photoluminescence of $Zr_{0.1}Al_{1.9}Mo_{2.9}V_{0.1}O_{12}$*

Jun-Ping Wang(王俊平)[1,2,†], Qing-Dong Chen(陈庆东)[1], Li-Gang Chen(陈立刚)[1], Yan-Jun Ji(纪延俊)[1], You-Wen Liu(刘友文)[2], and Er-Jun Liang(梁二军)[3]

[1] *Shandong Engineering Research Center of Aeronautical Materials and Devices; Key Laboratory of Aeronautical Optoelectronic Materials and Devices, College of Aeronautical Engineering, Binzhou University, Binzhou* 256603, *China*

[2] *College of Science, Nanjing University of Aeronautics and Astronautics, Nanjing* 210016, *China*

[3] *School of Physical Science & Engineering and Key Laboratory of Materials Physics of Ministry of Education, Zhengzhou University, Zhengzhou* 450052, *China*

(Received 31 July 2020; revised manuscript received 23 November 2020; accepted manuscript online 1 December 2020)

A new material of $Zr_{0.1}Al_{1.9}Mo_{2.9}V_{0.1}O_{12}$ is synthesized by the traditional solid state synthesis method. The phase transition, coefficient of thermal expansion, and luminescence properties of $Zr_{0.1}Al_{1.9}Mo_{2.9}V_{0.1}O_{12}$ are explored with Raman spectrometer, dilatometer, and x-ray diffraction (XRD) diffractometer. The results show that the $Zr_{0.1}Al_{1.9}Mo_{2.9}V_{0.1}O_{12}$ possesses the strong broad-band luminescence characteristics almost in the whole visible region. The sample is crystallized in a monoclinic structure group of $P2_1/a$ (No. 14) crystallized at room temperature (RT). The crystal is changed from monoclinic to orthorhombic structure when the temperature increases to 463 K. The material has very low thermal expansion performance in a wide temperature range. Its excellent low thermal expansion and strong pale green light properties in a wide temperature range suggest its potential applications in light-emitting diode (LED) and other optoelectronic devices.

Keywords: low thermal expansion, phase transition, x-ray diffraction (XRD), Raman spectrum, luminescence

PACS: 65.40.De, 81.05.Je, 61.50.–f, 78.30.–j **DOI:** 10.1088/1674-1056/abcf39

1. Introduction

The volume of material with positive expansion in nature expands with the increase of temperature. However, this property often leads to failure phenomena such as fatigue and fracture of materials, aging and falling off, and then limits its application in the fields of photoelectric communication, precision machinery, and other precision equipment materials. On the other hand, some materials have opposite properties: expanding when cooled and contracting when heated, and they are named negative thermal expansion materials (NTE). The finding of isotropic negative thermal expansion (NTE) material ZrW_2O_8 (0.3 K–1050 K) in a large temperature range illuminates the way to regulate the expansion coefficient of engineering materials.[1] The negative expansion material has attracted more and more attention due to its special scientific research and application value. At present, the negative expansion materials are the AM_2O_7 series represented by ZrV_2O_7,[2] the series of magnetic materials represented by Mn_3GaN,[3] the $A(CN)_2$ series represented by $Zn(CN)_2$,[4] the zeolite series represented by siderolite,[5] the two-dimensional graphite as the representative of graphite.[6] In 1997, a rare-earth tungstate or molybdate negative thermal expansion material with $A_2M_3O_{12}$ (A denotes a valence transition metal, M refers to Mo or W) was reported as chemical general formula and negative thermal expansion materials of vanadate series.[7–10] Among the negative thermal expansion materials with frame structure, $A_2M_3O_{12}$ series materials are the most stable and widely studied materials. However, the application of $A_2M_3O_{12}$ series is restricted by two main problems: hygroscopicity and phase transformation.[11–15] In order to solve these two problems, substitutions of tervalent transition elements for A of $A_2M_3O_{12}$ were performed.[16–27] On the basis of the $A_2M_3O_{12}$ materials, the trivalent elements at site A were replaced by tetravalent elements and the hexavalent ions at site M were partly replaced by pentavalent ions in order to maintain the valence balance. After the elements at sites A and M in $A_2M_3O_{12}$ were replaced with the ions with the same or different valences, the expansion coefficient was significantly changed and the phase transition temperature decreased.[28–30] The $ZrScMo_2VO_{12}$,[29] $HfScMo_2VO_{12}$,[31] and $HfScW_2PO_{12}$[32] were designed and they exhibited not only NTE in a relatively wide temperature range but also intense broad-band photoluminescence (PL) covering the visible range. In this study a novel material $Zr_{0.1}Al_{1.9}Mo_{2.9}V_{0.1}O_{12}$ is prepared by the solid-phase sintering process and is crystallized into a monoclinic structure group of $P2_1/a$ (No. 14)

*Project supported by the National Natural Science Foundation of China (Grant Nos. 11874328, U1731121, and 41401384) and the Shandong Province Higher Educational Science and Technology Program, China (Grant No. J17KB127).

†Corresponding author. E-mail: Wangjunping-99@163.com

© 2021 Chinese Physical Society and IOP Publishing Ltd

at room temperature (RT). The material shows the better low thermal expansion (LTE) property and the strong broad-band luminescence in almost the whole visible region. Its LTE and white light properties in a wide temperature range suggeste its potential applications in light-emitting diode (LED) and other optoelectronic devices.

2. Experimental procedure

The $Zr_{0.1}Al_{1.9}Mo_{2.9}V_{0.1}O_{12}$ was prepared by the solid-phase sintering process with ZrO_2 (in purity 99%), Al_2O_3 (99%), MoO_3 (99%), and V_2O_5 (99%) according to the molar ratios of elements. The raw materials were first mixed and ground for 2 h and then pressed into pieces with a thickness of about 10 mm and a diameter of 3 mm–10 mm. After the high-temperature furnace was heated to 973 K, the samples were plased into the furnace, heated for 5 h, and then cooled to RT in the furnace. The samples were sintered twice under the same conditions to obtain target products.

3. Results

3.1. Crystal structure analysis

The crystal structure and lattice constants were obtained from the refinements of x-ray diffraction (XRD) patterns with the Rietveld method (Fig. 1). The result shows that $Zr_{0.1}Al_{1.9}Mo_{2.9}V_{0.1}O_{12}$ possesses a monoclinic structure with space group $P2_1/a$ (ICSD 01-084-1652) at RT. The refined cell parameters of $Zr_{0.1}Al_{1.9}Mo_{2.9}V_{0.1}O_{12}$ are as follows: $a = 15.386$ Å, $b = 9.042$ Å, $c = 17.875$ Å, $V = 1014.322$ Å^3, $\alpha = 90°$, $\beta = 125.457°$, $\gamma = 90°$, $R_{exp} = 2.82\%$, and $R_{wp} = 8.24\%$, $R_p = 5.88\%$.

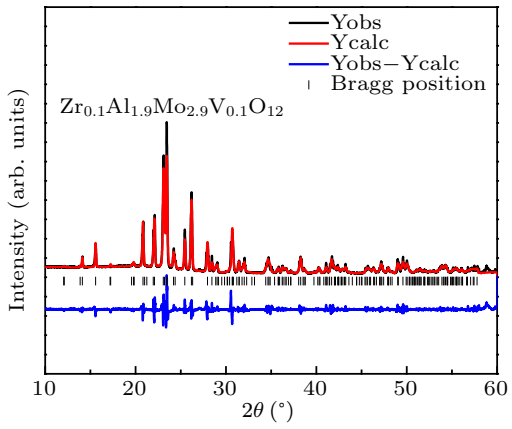


Fig. 1. The results of the Rietveld analysis of the XRD pattern for $Zr_{0.1}Al_{1.9}Mo_{2.9}V_{0.1}O_{12}$.

Figure 2 shows the Raman spectra of $Al_2Mo_3O_{12}$ and $Zr_{0.1}Al_{1.9}Mo_{2.9}V_{0.1}O_{12}$ at RT. From the figure we can see the variations of Raman vibration modes with the doping of Zr^{4+} ions and V^{5+} ions. The Raman peaks at 1050 cm^{-1}–900 cm^{-1} are ascribed to the internal symmetric stretching vibration (ν_1) of the MoO_4 or VO_4 tetrahedron. The Raman peaks at 900 cm^{-1}–750 cm^{-1} are attributed to the asymmetric stretching vibration (ν_3) of the MoO_4 or VO_4 tetrahedron. The Raman peaks at 400 cm^{-1}–320 cm^{-1} are arise from the bending vibrations (ν_2 and ν_4) of the MoO_4 or VO_4 tetrahedron, and those peaks below 300 cm^{-1} are stemed from the translational and librational motions of the AlO_6 or ZrO_6 polyhedron.[33–35] There are obvious changes in the Raman spectra of $Zr_{0.1}Al_{1.9}Mo_{2.9}V_{0.1}O_{12}$ that the Raman peaks at 662 cm^{-1} and 975.91 cm^{-1} disappear, but the new Raman peaks at 747 cm^{-1} and 947.7 cm^{-1} appear. The Zr^{4+} /V^{5+} ion substitution promotes the lattice and asymmetric stretching vibrations of $Al_2Mo_3O_{12}$, and the thermal change in Mo–O distance in the lattice, results in the shift of the Raman peak.

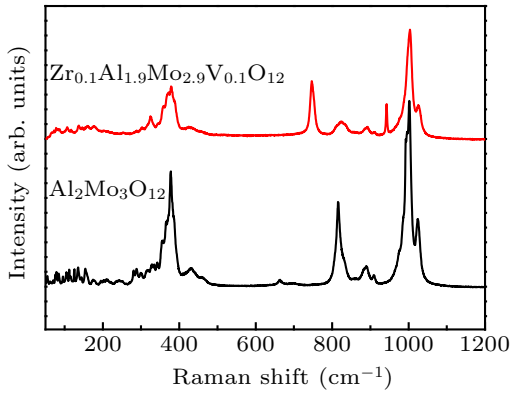


Fig. 2. Raman spectra of (a) $Zr_{0.1}Al_{1.9}Mo_{2.9}V_{0.1}O_{12}$ and (b) $Al_2Mo_3O_{12}$.

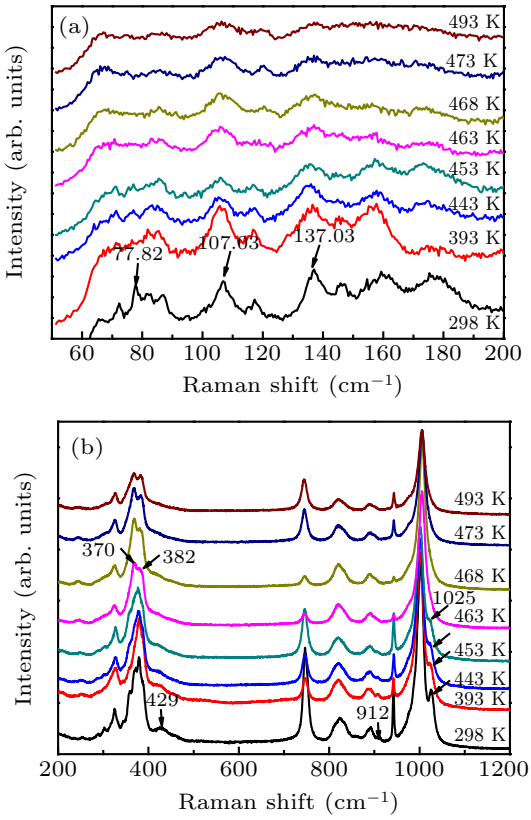


Fig. 3. Temperature-dependent Raman spectra of $Zr_{0.1}Al_{1.9}Mo_{2.9}V_{0.1}O_{12}$ from (a) 50 cm^{-1} to 200 cm^{-1} and (b) 200 cm^{-1} to 1200 cm^{-1}.

The Raman spectra can be used to sensitively distinguish the structural changes of $A_2M_3O_{12}$ from monoclinic phase to orthorhombic phase. For analyzing the structure of $Zr_{0.1}Al_{1.9}Mo_{2.9}V_{0.1}O_{12}$ at low temperature and determining its phase transition temperature, we measure the Raman spectra of $Zr_{0.1}Al_{1.9}Mo_{2.9}VO_{12}$ from 298 K to 493 K. It can be seen that the Raman spectra of $Zr_{0.1}Al_{1.9}Mo_{2.9}VO_{12}$ are basically unchanged from 298 K to 453 K from Fig. 3. When the temperature reaches 463 K, the Raman spectrum peak at 1025 cm^{-1} which is the characteristic Raman peak of monoclinic structure, disappears. The Raman peak at 380 cm^{-1} gradually splits into two peaks at 370 cm^{-1} and 382 cm^{-1}. These changes further indicate that the monoclinic structure of $Zr_{0.1}Al_{1.9}Mo_{2.9}V_{0.1}O_{12}$ is maintained until the temperature increases to at least 463 K. The crystal of $Zr_{0.1}Al_{1.9}Mo_{2.9}V_{0.1}O_{12}$ changes from monoclinic to orthorhombic structure phase at about 463 K.

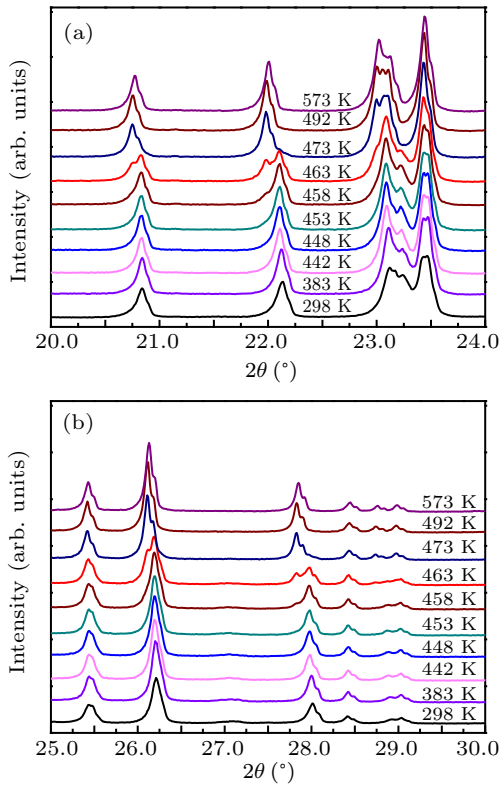


Fig. 4. (a) XRD patterns of $Zr_{0.1}Al_{1.9}Mo_{2.9}V_{0.1}O_{12}$ at different temperatures, and (b) their partial magnification.

The variable temperature XRD measurements of sample at different temperatures are used to explore the LTE property and structural transformation of $Zr_{0.1}Al_{1.9}Mo_{2.9}V_{0.1}O_{12}$. The experimental results are shown in Fig. 4. The diffraction peak near 25° is considered as the characteristic diffraction peak of $Zr_{0.1}Al_{1.9}Mo_{2.9}V_{0.1}O_{12}$ with a monoclinic structure. With the increase in temperature, the intensity of the diffraction peak near 25° decreases gradually until it disappears completely when the temperature goes up to at least 463 K, which is shown in Fig. 4(b). It can also be seen that the diffraction peaks at 22.11° and 27.96° are significantly changed at 463 K. These results further show that the lattice constant of $Zr_{0.1}Al_{1.9}Mo_{2.9}V_{0.1}O_{12}$ material changes at 463 K. The result is consistent with the dilatometer and high-temperature Raman spectrum results, indicating that the $Zr_{0.1}Al_{1.9}Mo_{2.9}V_{0.1}O_{12}$ exhibits the orthorhombic phase at 463 K.

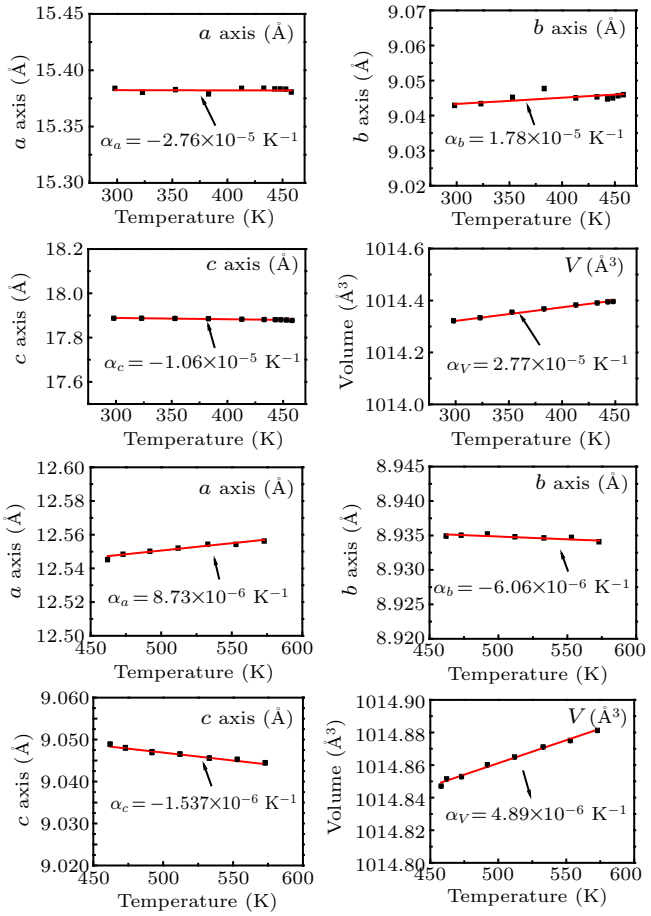


Fig. 5. Variations of lattice constants and cell volume with temperature of $Zr_{0.1}Al_{1.9}Mo_{2.9}V_{0.1}O_{12}$ at temperature ranging from RT to 600 K.

Lattice constants and volumes of $Zr_{0.1}Al_{1.9}Mo_{2.9}V_{0.1}O_{12}$ under different temperatures are calculated based on Rietveld analysis (Fig. 5). The tested temperature in a ranged of 300 K–463 K (phase transition temperature) and 463 K–673 K. The thermal expansion coefficients of a, b, and c axes from 300 K to 463 K are calculated to be $\alpha_a = -2.16\times10^{-5}$ K^{-1}, $\alpha_b = 1.78\times10^{-5}$ K^{-1}, and $\alpha_c = -1.06\times10^{-5}$ K^{-1}, respectively. The volume thermal expansion coefficient $\alpha_V = 2.77\times10^{-5}$ K^{-1} and the linear thermal expansion coefficient $\alpha_l = \alpha_V/3 = 9.23\times10^{-6}$ K^{-1} from 300 K to 463 K. When the temperature increases to 463 K, the $Zr_{0.1}Al_{1.9}Mo_{2.9}V_{0.1}O_{12}$ changes from monoclinic phase to orthorhombic phase. The coefficient of thermal expansion (CTE) of $Zr_{0.1}Al_{1.9}Mo_{2.9}V_{0.1}O_{12}$ from 463 K to 600 K are calculated to be $\alpha_a = 8.73\times10^{-6}$ K^{-1}, $\alpha_b = -6.06\times10^{-6}$ K^{-1}, $\alpha_c = -1.53\times10^{-6}$ K^{-1}, $\alpha_V = 4.89\times10^{-6}$ K^{-1}, and $\alpha_l = \alpha_V/3 = 1.63\times10^{-6}$ K^{-1},

respectively. The $Zr_{0.1}Al_{1.9}Mo_{2.9}V_{0.1}O_{12}$ has good LTE performance from 463 K to 600 K.

The $Zr_{0.1}Al_{1.9}Mo_{2.9}V_{0.1}O_{12}$ can be considered as a deformation of $Al_2Mo_3O_{12}$ by replacing Al^{3+} with Zr^{4+} and replacing Mo^{6+} with V^{5+} in order to maintain charge balance. The orthorhombic $Zr_{0.1}Al_{1.9}Mo_{2.9}V_{0.1}O_{12}$ is a frame work structure with corner-shared ZrO_6/AlO_6 octahedron and VO_4/MoO_4 tetrahedron. Each ZrO_6/AlO_6 octahedron shares all the angles with six VO_4/MoO_4 tetrahedrons and each VO_4/MoO_4 tetrahedron shares all the angles with four ZrO_6/AlO_6 octahedrons. The negative thermal expansion of orthorhombic structure is caused by bending the *M*–O–*A* bond. The transverse vibration of bridge oxygen atom leads the *M*–O–*A* chain to be bent. The phase transition temperature and thermal expansion property of $Zr_{0.1}Al_{1.9}Mo_{2.9}V_{0.1}O_{12}$ are related to the electronegativity of cations. The electronegativity of Zr^{4+} (1.33 Pauling) is lower than that of Al^{3+} (1.61 Pauling), and the electronegativity of V^{5+} (1.63 Pauling) is lower than that of Mo^{6+} (1.8 Pauling). The zero thermal expansion (ZTE) and variation of CTE are attributed to the difference in electronegativity between Zr^{4+}/V^{5+} and Al^{3+}/Mo^{6+}. Once Zr^{4+}/V^{5+} replaced Al^{3+}/Mo^{6+} ions in the lattice, the balance among the surrounding six MoO_4 tetrahedron electron clouds is broken. The effective negative charge of oxygen anioninc reases, thus resulting in the increase in oxygen-oxygen repulsion. So the attraction to the surrounding MoO_4 (VO_4) tetrahedron is weak and the Mo–O bond is strengthened to form a harder polyhedron. The bending degree of the Al–O–Mo (V) or Al (Zr)–O–Mo bond is less than that of the Al–O–Mo bond, thus $Zr_{0.1}Al_{1.9}Mo_{2.9}V_{0.1}O_{12}$ exhibits the better LTE property.

3.2. Thermal expansion characteristic

The LTE property of $Zr_{0.1}Al_{1.9}Mo_{2.9}V_{0.1}O_{12}$ is studied by dilatometer. Figure 6 shows the variation of the relative length of $Zr_{0.1}Al_{1.9}Mo_{2.9}V_{0.1}O_{12}$ cylinder with temperature from 298 K to 700 K. The phase transition temperature of $Zr_{0.1}Al_{1.9}Mo_{2.9}V_{0.1}O_{12}$ is about 463 K. The CTE of $Zr_{0.1}Al_{1.9}Mo_{2.9}V_{0.1}O_{12}$ is obtained to be 2.17×10^{-6} K^{-1} from 463 K to 781 K and exhibits the LTE property. The results are well consistent with the XRD measurements at different temperatures. The variation of the relative length measured by a dilatometer could sensitively reflect the phase transformation and the release process of crystal water. The very smooth linear thermal expansion curve in Fig. 6 shows that the material has no hygroscopicity from 298 K to 700 K.

The linear expansion coefficient calculated by the XRD patterns at different temperatures is slightly larger than that directly measured with the dilatometer. The CTE calculated with the XRD patterns at different temperatures reflects the intrinsic thermal expansion of crystal cells, whereas the dilatometer measures the macroscopic expansion coefficient of the bulk sample. The microstructure has a certain influence on the thermal expansion of block material. The linear CTE calculated with the variable temperature XRD patterns is slightly larger than that measured with the dilatometer, indicating that the external effect has the negative contribution to the linear CTE.

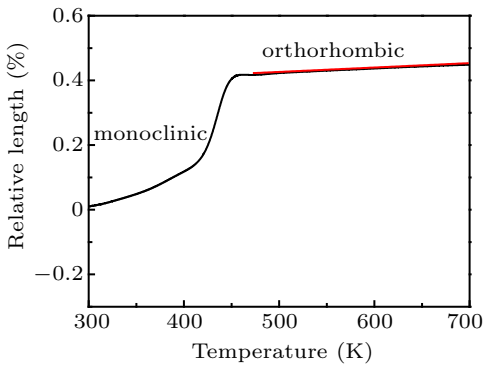


Fig. 6. The variation of the relative length with temperatures of $Zr_{0.1}Al_{1.9}Mo_{2.9}V_{0.1}O_{12}$.

In order to explore the hydroscopicity of the material, the thermal analysis test is carried out for $Zr_{0.1}Al_{1.9}Mo_{2.9}V_{0.1}O_{12}$. Figure 7 shows the thermo gravimetry (TG)/digital security controls (DSC) curve from RT to 873 K. It can be seen that the TG curve of the sample and the weight of the sample have no change basically in a temperature range from about 300 K to 873 K. The results further illustrate that the $Zr_{0.1}Al_{1.9}Mo_{2.9}V_{0.1}O_{12}$ has no water absorption. There is an exothermic peak at 463.33 K, which indicates that the $Zr_{0.1}Al_{1.9}Mo_{2.9}V_{0.1}O_{12}$ changes from monoclinic phase to orthorhombic phase at 463.33 K, which is consistent with the previous result of the XRD and the Raman analysis at different temperatures.

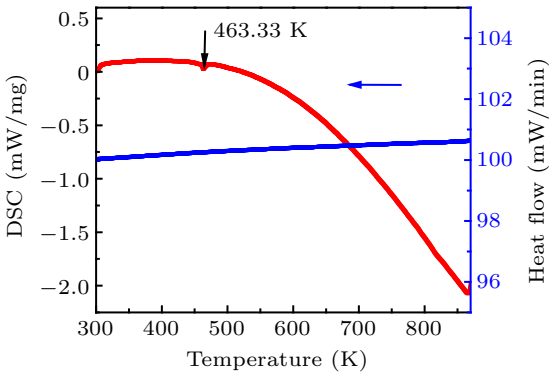


Fig. 7. The curve of the DSC and heat flow *versus* temperatures of $Zr_{0.1}Al_{1.9}Mo_{2.9}V_{0.1}O_{12}$ in a temperature range from RT to 873 K.

Figure 8(a) shows the image of scanning electron microscope (SEM) of $Zr_{0.1}Al_{1.9}Mo_{2.9}V_{0.1}O_{12}$. Figures 8(b)–8(d) display the energy dispersive spectrometer (EDS) spectra at the corresponding locations. Most of samples are composed of polyhedrons with good crystallinity (Fig. 8(a)). Table 1 shows

the content of Al, Zr, Mo, V, and O elements (%). From Fig. 8 and Table 1, it can be seen that the $Zr_{0.1}Al_{1.9}Mo_{2.9}V_{0.1}O_{12}$ contains only five elements of Al, Zr, Mo, V, and O and there are no other impurity elements. The element ratio in the sample is close to the molar ratio of elements in the compound $Zr_{0.1}Al_{1.9}Mo_{2.9}V_{0.1}O_{12}$.

The density of $Zr_{0.1}Al_{1.9}Mo_{2.9}V_{0.1}O_{12}$ is measured by the Archimedes drainage method. The density of $Zr_{0.1}Al_{1.9}Mo_{2.9}V_{0.1}O_{12}$ synthesized by solid-state sintering is 3.52 g/cm^3 and its theoretical density is 3.24 g/cm^3. The compactness of the composite can increase and reach 92.05%. Comparing with the above XRD analysis, it can be seen that $Zr_{0.1}Al_{1.9}Mo_{2.9}V_{0.1}O_{12}$ has high purity and density.

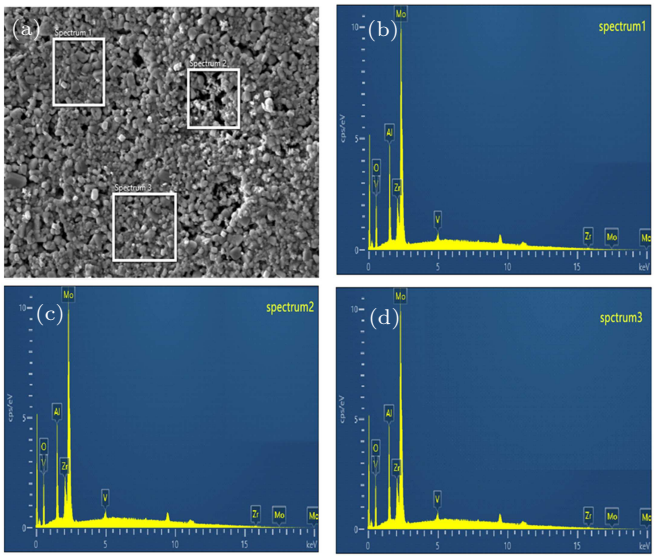


Fig. 8. (a) SEM image and ((b)–(d)) energy dispersive spectrometer results of $Zr_{0.1}Al_{1.9}Mo_{2.9}V_{0.1}O_{12}$.

Table 1. Atomic ratios of O, Al, V, Zr, and Mo at three positions in $Zr_{0.1}Al_{1.9}Mo_{2.9}V_{0.1}O_{12}$ (%).

Element	O	Al	V	Zr	Mo
Atomic ratios (%)	35.88	9.57	1.01	1.68	51.67
Atomic ratios (%)	35.91	9.61	0.98	1.72	51.78
Atomic ratios (%)	35.83	9.58	0.95	1.73	51.91

3.3. Luminescence mechanism of $Zr_{0.1}Al_{1.9}Mo_{2.9}V_{0.1}O_{12}$

Figure 9 shows the UV visible absorption spectra of $Zr_{0.1}Al_{1.9}Mo_{2.9}V_{0.1}O_{12}$ at RT and corresponding calculated bandgap. The peak value of the UV absorption spectrum around 280 nm and the optical bandgap can be estimated with the UV absorption spectrum according to Tauc equation as follows:[36]

$$(\alpha h\nu)^2 = \mathrm{A}\left(h\nu - E_\mathrm{g}\right), \tag{1}$$

where α is the absorption coefficient, h is the Planck constant, and A is the proportional constant. The bandgap of the material can be calculated from Fig. 9(b). The band gap of $Zr_{0.1}Al_{1.9}Mo_{2.9}V_{0.1}O_{12}$ at RT is calculated to be 2.75 eV.

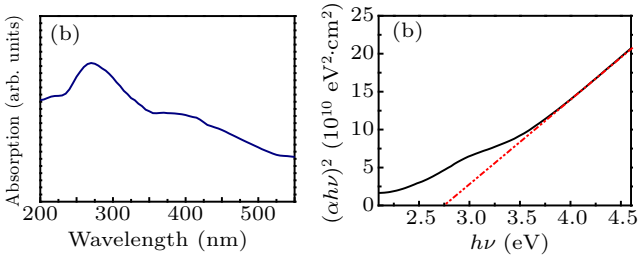


Fig. 9. (a) UV-vis absorption spectrum at RT, and (b) band gap estimation from absorption spectrum of $Zr_{0.1}Al_{1.9}Mo_{2.9}V_{0.1}O_{12}$.

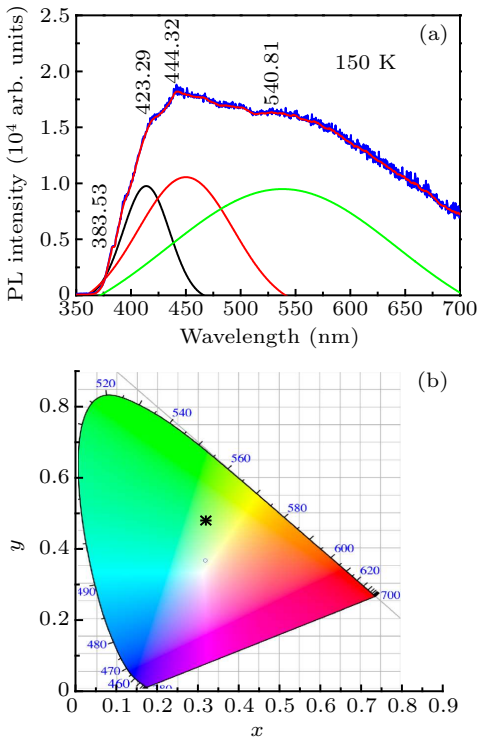


Fig. 10. (a) PL spectra of $Zr_{0.1}Al_{1.9}Mo_{2.9}V_{0.1}O_{12}$ with 295-nm excitation at 150 K (PL spectrum deconvolution into two narrow and one broad bands), and (b) commission Internationale de l'Eclairage (CIE) chromaticity coordinates of PL.

The PL spectra of $Zr_{0.1}Al_{1.9}Mo_{2.9}V_{0.3}O_{12}$ are investigated by photoluminescence spectra under the excitation of 295 nm at 150 K (Fig. 10). The PL spectrum could be deconvoluted into three narrow bands and one broad band. The narrow emission peaks are located at 383.53 nm, 423.29 nm, and 444.32 nm, while the other wide emission peak is located at 540.81 nm. The material emits strong pale green light and the clear visible light, which can be observed with naked eyes. The $Zr_{0.1}Al_{1.9}Mo_{2.9}V_{0.3}O_{12}$ exhibits very strong wide band luminescence characteristic from 370 nm to 650 nm covering almost the whole visible light region. In order to visually observe the luminescence performance of $Zr_{0.1}Al_{1.9}Mo_{2.9}V_{0.1}O_{12}$ at RT, we draw the color coordinates under different doping conditions. As can be seen from Fig. 10(b) that the Commission Internationale de l'Eclairage (CIE) chromaticity coordinates of $Zr_{0.1}Al_{1.9}Mo_{2.9}V_{0.1}O_{12}$ are located in the green region.

Figure 11 shows that the three narrow luminous peaks basically remaining unchanged and the wide spectrum at 540.81 nm has a significant blue shift with the increase in temperature. This is because the interaction between donor and acceptor pair of monoclinic phase truns to relate to the distance between them with the decrease of temperature. Because the donor acceptor pairs have different distances, there appear different interaction intensities between donors and acceptors located in the center of polyhedron in the lattice, which may be the reason for the broadening of fluorescence peak. The very strong photoluminescence spectrum of the material is the intrinsic luminescence of the material itself, which implies that there is a direct band gap in the material.

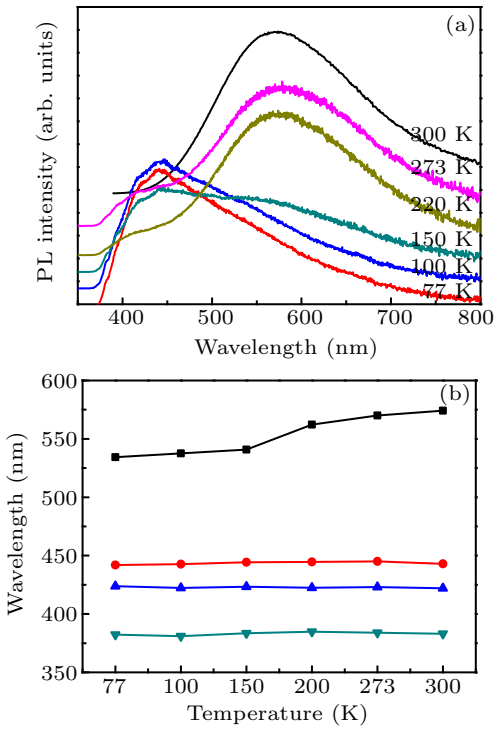


Fig. 11. (a) PL spectra of $Zr_{0.1}Al_{1.9}Mo_{2.9}V_{0.1}O_{12}$ at different temperatures and (b) position of PL peak varying with temperature.

The PL spectra of $Zr_xAl_{2-x}Mo_{3-x}V_xO_{12}$ ($x = 0.0$, 0.1, 0.2, 0.3, and 0.4) are investigated under the excitation of 295 nm (Fig. 12). The $Zr_xAl_{2-x}Mo_{3-x}V_xO_{12}$ ($x = 0.0$, 0.1, 0.2, 0.3, and 0.4) exhibit strong broad-band luminescence characteristics. The luminescence wavelengths range from 370 nm to 650 nm, covering almost the whole visible region. A wide green emission band occurs at 530 nm, and the luminescence intensity becomes stronger with the increase in doping amount.

Previous studies have found that the luminescence of $A_2M_3O_{12}$ series material was very weak. The optical properties of the material are improved by doping Zr^{4+} and V^{5+} ions, and the materials emit strong light over a wide temperature range. The abundant physical energy of the material $Zr_{0.1}Al_{1.9}Mo_{2.9}V_{0.1}O_{12}$ is ascribed to its special structure. The strong multi-band luminescence is attributed to the co-doping effect of n-type and p-type based on $Al_2Mo_3O_{12}$. One Al^{3+} ion in $Al_2Mo_3O_{12}$ is replaced by one Zr^{4+} ion, and Mo^{6+} ion is replaced by a V^{5+} ion to maintain the balance of charge. This substitution triggers the functions of n-type and p-type co-doping in semiconductors. The n-type doping and p-type doping generate donor state (D) and acceptor state (A) between valence band (VB) and conduction band (CB), respectively. It can be inferred that the fluorescence peak at 383.53 nm corresponds to the band side transition from CB to VB, the fluorescence peak at 423.29 nm and 444.32 nm correspond to the transition from CB to acceptor level (EA) and from donor level (ED) to VB, respectively, and the wide emission peak near the wide band at 540.81 nm which is dependent on the change of temperature, can be mainly attributed to the energy level transition of donor acceptor pair (DAP).

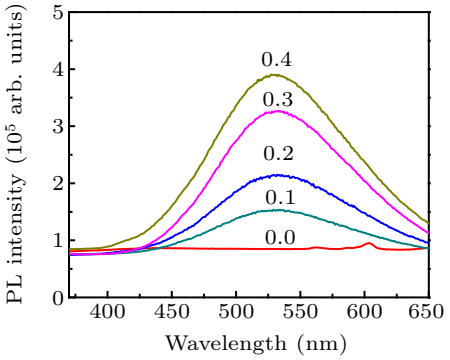


Fig. 12. PL spectra of $Zr_xAl_{2-x}Mo_{3-x}V_xO_{12}$ ($x = 0$, 0.1, 0.2, 0.3, and 0.4) under 295-nm excitation.

The interaction between donor acceptor pairs is related to the size of their spacing, because there are donor acceptor pairs with different spacings, they are located in different polyhedral centers in the lattice. There are different intensities between the donor and the acceptor, which might be the reason for broadening the fluorescence peak. The distance between donor and acceptor changes with temperatures. According to the basic characteristics of donor acceptor pair luminescence, the shift of DAP peaks with temperature rising can be explained by the following equation:

$$E_{\mathrm{L}}(r) = E_{\mathrm{L}}(\mathrm{r}) = E_{\mathrm{i}} - E_{\mathrm{f}} = E_{\mathrm{g}} - (E_{\mathrm{A}} + E_{\mathrm{D}}) + \frac{e^2}{4\pi\varepsilon_0\varepsilon_{\mathrm{r}} r}. \quad (2)$$

Equation (2) shows that different DAP has a different distance, and the energy of photon emitted is also different. In Eq. (2), E_{g} is the band gap of semiconductor, E_{D} and E_{A} are the binding energies of donor and acceptor respectively, ε_{r} is the static field dielectric coefficient of crystal, and r is the distance between donor and acceptor. With the decrease of temperature, $Zr_{0.1}Al_{1.9}Mo_{2.9}V_{0.1}O_{12}$ has a monoclinc structure at low temperature, and the material exhibits positive thermal expansion characteristics. With the decrease of temperature, the distance between donor and recipient becomes smaller, and the luminous energy moves towards the direction of high energy, so the luminous peak at 540.81 nm is blue-shifted.

4. Conclusions

A new kind of novel material $Zr_{0.1}Al_{1.9}Mo_{2.9}V_{0.1}O_{12}$ is synthesized by the traditional high temperature solid synthesis method. This material shows an excellent LTE property in a wide temperature range and has strong broad band luminescence covering almost the whole visible region. Structure analysis shows that $Zr_{0.1}Al_{1.9}Mo_{2.9}V_{0.1}O_{12}$ is crystallized into a monoclinic structure group of $P2_1/a$ (No. 14) at RT and changes from monoclinic phase to orthorhombic phase belonging to the group of *Pbcn* (No. 60) at 463 K. The Al^{3+} and Mo^{6+} are replaced in $Al_2Mo_3O_{12,}$ respectively, by Zr^{4+} and V^{5+}, resulting in $Zr_{0.1}Al_{1.9}Mo_{2.9}V_{0.1}O_{12}$ that exhibits the lower anisotropy in orthorhombic phase and shows an LTE over a wide temperature range. Its excellent LTE and pale green light properties in a wide temperature range indicate its potential applications in LED and other optoelectronic devices. Meanwhile, this co-doping effect generates the unique electronic property and lays the foundation for further studying its special optical and electrical properties.

References

[1] Mary T A, Evans J S O, Vogt T and Sleight A W 1996 *Science* **272** 90
[2] Wang J P, Chen Q D, Li S L, Ji Y J, Mu W Y, Feng W W, Zeng G J, Liu Y W and Liang E J 2018 *Chin. Phys. B* **27** 066501
[3] Sun Y, Wang C, Wen Y C and Chu L H 2010 *J. Am. Ceram. Soc.* **93** 650
[4] Ding P, Liang E J, Jia Y and Du Z Y 2008 *J. Phys.: Condens. Matter* **20** 275224
[5] Suleimanov R A and Abdullaev 1993 *Carbon* **31** 1011
[6] Deng Z, Smolyanitsky A, Li Q, Feng X Q and Cannara R J 2012 *Nat. Mater.* **11** 1032
[7] Liu H, Sun W, Zhang Z, Zhou M, Meng X and Zeng X 2018 *J. Alloys Compd.* **751** 49
[8] Prisco L P, Marzano M, Ponton P I and Costa A M L M 2019 *Int. J. Appl. Cera.* **16** 13054
[9] Mary T A and Sleight A W J 1999 *Mater. Res.* **14** 912
[10] Evans J S O, Mary T A and Sleight A W 1997 *J. Solid State Chem.* **133** 580
[11] Gao S, Zhao N, Liu Q and Li Y 2019 *J. Alloys Compd.* **779** 108
[12] Varga T, Moats J L, Ushakov S V and Navrotsky A 2007 *J. Mater. Res.* **22** 2512
[13] Prisco L P, Romao C P, Rizzo F, White M A and Marinkovic B A 2013 *J. Mater. Sci.* **48** 2986
[14] Cheng Y G, Liu X S, Chen H J, Chao M J and Liang E J 2015 *Phys. Chem. Chem. Phys.* **17** 10363
[15] Ari M, Miller K J, Marinkovic B A, Jardim P M, Avillez R, Rizzo F and White M A 2011 *J. Sol-Gel Sci. Techn.* **58** 121
[16] Yuan H, Wang C, Gao Q L, Ge X, Sun H, Lapidus S H, Guo J, Chao M, Jia Y and Liang E J 2020 *Inorg. Chem.* **59** 4090
[17] He X H, Qi H, Xu Q, Liu X S, Xu L and Yuan B H 2019 *Chin. Phy. B* **28** 056501
[18] Li Z Y, Song W B and Liang E J 2011 *J. Phys. Chem. C* **115** 17806
[19] Liu Y, Yuan B, Cheng Y, Liang E J, Ge X, Yuan H, Zhang Y, Guo J and Chao M J 2018 *Mater. Res. Bull.* **99** 255
[20] Xiao X, Zhou W, Liu X, Chao M J, Li Y, Zhang N, Liu Y, Li Y, Feng D and Liang E J 2015 *Ceram. Int.* **41** 2361
[21] Liu X S, ChengY G, Yuan B H, Liang E J and Zhang W F 2019 *Chin. Phy. B* **28** 096501
[22] Miller K J, Romao C P, Bieringer M, Marinkovic B A, Prisco A and White M 2012 *J. Am. Chem. Soc.* **96** 561
[23] Cheng Y, Xiao X, Liu X, Wu M M, Peng J and Hu Z B 2013 *Physica B* **411** 173
[24] Truitt R, Hermes I M, Main A, Sendecki A and Lind C 2015 *Materials* **8** 700
[25] Cheng Y, Liang Y, Mao Y, Ge Xi, Yuan B, Guo Juan, Chao M J and Liang E J 2017 *Mater. Res. Bull.* **85** 176
[26] Liu X S, Ge X H, Liang E J and Zhang W F 2017 *Chin. Phys. B* **26** 118101
[27] Liu H, Wang X, Zhang Z, Zhang Z ang Chen X 2012 *Ceram. Int.* **38** 6349
[28] Li Q, Yuan B, Liang E J, Song W, Liang E J and Yuan B 2012 *Chin. Phys. B* **21** 046501
[29] Ge X H, Mao Y C, Liu X S, Chen Y G, Yuan B H, Chao M J and Liang E J 2016 *Sci. Rep.* **6** 24832
[30] Chen D, Yuan B and Cheng Y 2016 *Phys. Lett. A* **380** 4070
[31] ChengY G, Liang Y, Ge X H, Liu X S, Yuan B H, Guo J, Chao M J and Liang E J 2016 *RSC Adv.* **6** 53657
[32] ChengY G, Liang Y, Mao Y C, Ge X H, Yuan B H, Guo J, Chao M J and Liang E J 2017 *Mater. Res. Bull.* **85** 176
[33] Schulz B, Andersen H, Al Bahri O O K and Johannessen B 2018 *CrystEngComm* **20** 1352
[34] Surjith A, James N K and Ratheesh R 2011 *J. Alloys Compd.* **509** 9992
[35] Yanase I, Ootomo R and Kobayashi H 2018 *J. Therm. Anal. Calorim.* **132** 1
[36] Husain S, Alkhtaby L A, Giorgetti E, Zoppi A and Miranda M M 2016 *J. Lumin.* **172** 258